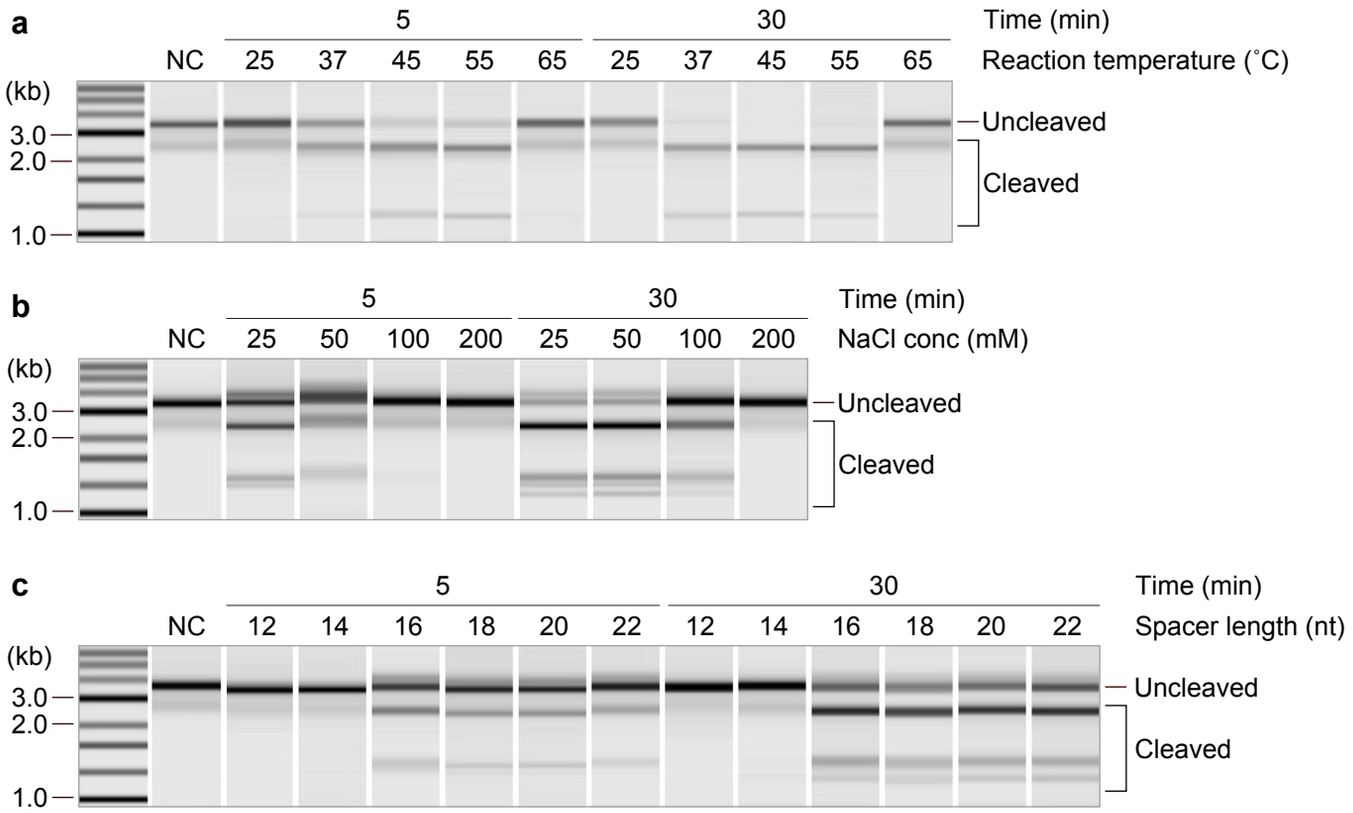

Supplementary Fig. 1 | In vitro target DNA cleavage by Casλ2.
(**a–c**) Representative electropherograms of DNA cleavage products generated under different temperature (**a**), NaCl concentration (**b**), and spacer length (**c**) conditions, analyzed by MultiNA microchip electrophoresis.

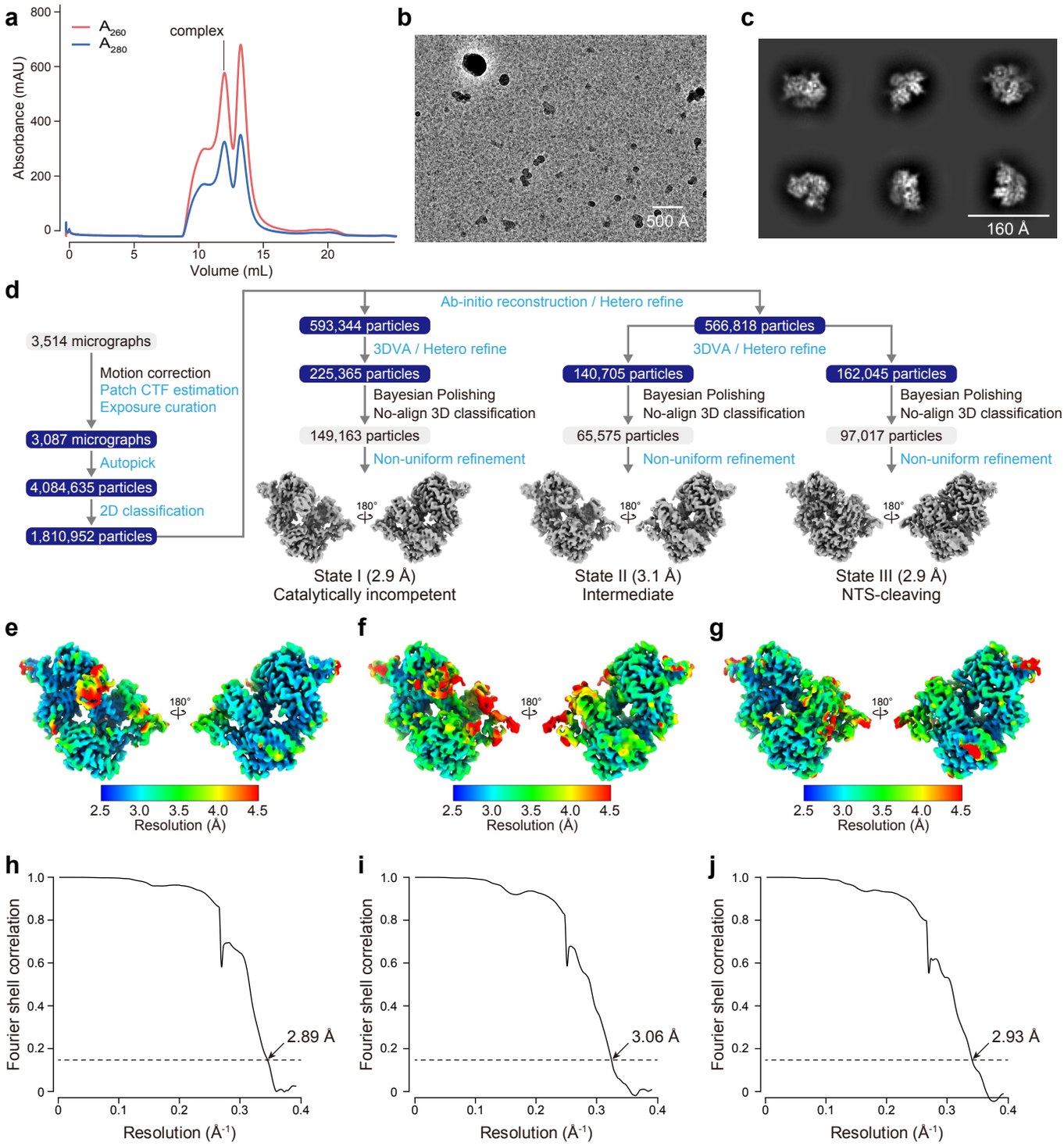

Supplementary Fig. 2 | Single-particle cryo-EM analysis of the CasλΔ2–crRNA–target DNA ternary complex.
(a) Size-exclusion chromatography profile of the CasλΔ2–crRNA–target DNA complex. The peak fraction indicated as the complex was used for the following cryo-EM analyses.
(b) Representative cryo-EM micrograph, recorded on a 300-kV Titan Krios microscope with a K3 camera.
(c) Representative 2D class average images.
(d) Single-particle cryo-EM image processing workflow. The data processing done in cryoSPARC is shown in blue, while the processing done in RELION is shown in black.
(e–g) Cryo-EM density maps of the CasλΔ2–crRNA–target DNA complexes in the catalytically incompetent (**e**), intermediate (**f**), and NTS-cleaving (**g**) states, according to the local resolution.
(h–j) Fourier shell correlation curves for the 3D reconstructions of the CasλΔ2–crRNA–target DNA complexes in the catalytically incompetent (**h**), intermediate (**i**), and NTS-cleaving (**j**) states.

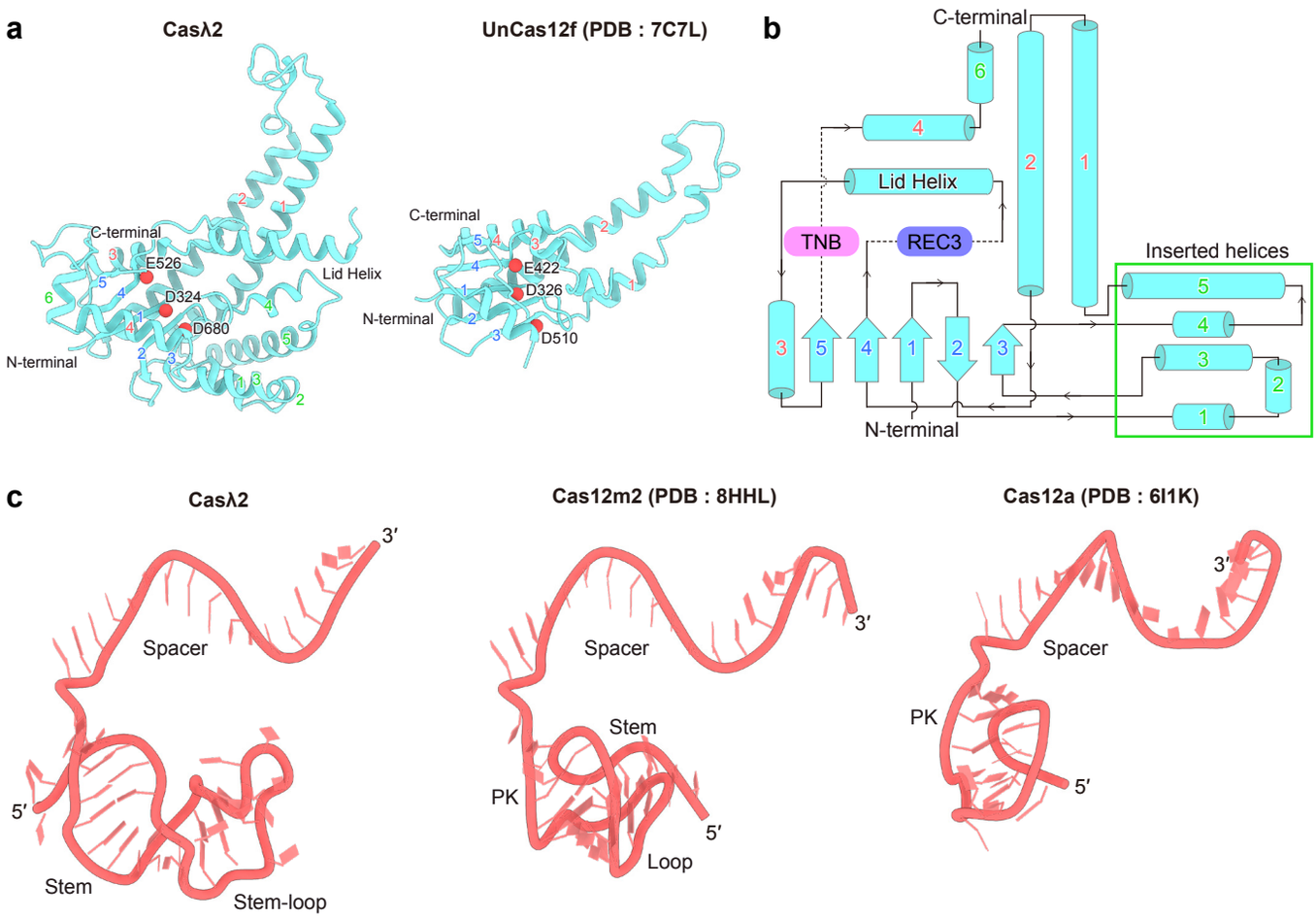

Supplementary Fig. 3 | RuvC domain and crRNA structures.
(a) The RuvC domain structure of CasΛ2 and that of UnCas12f (PDB: 7C7L). The RuvC domains comprise the RNaseH fold. The conserved β strands and α helices are numbered in blue and red, respectively, while the additional helices observed in CasΛ2 are numbered in green. The conserved RuvC active site is indicated as red spheres.
(b) Schematic of the RuvC domain of CasΛ2.
(c) Structures of crRNAs of CasΛ2 (left), Cas12m2 (center) (PDB: 8HHL), and Cas12a (right) (PDB: 6I1K). While the crRNAs of most of the Cas12 enzymes, including Cas12m2 and Cas12a, comprise the conserved pseudoknot structure, the crRNA of CasΛ2 comprises the stem and stem-loop, but lacks the pseudoknot structure. PK, pseudoknot.

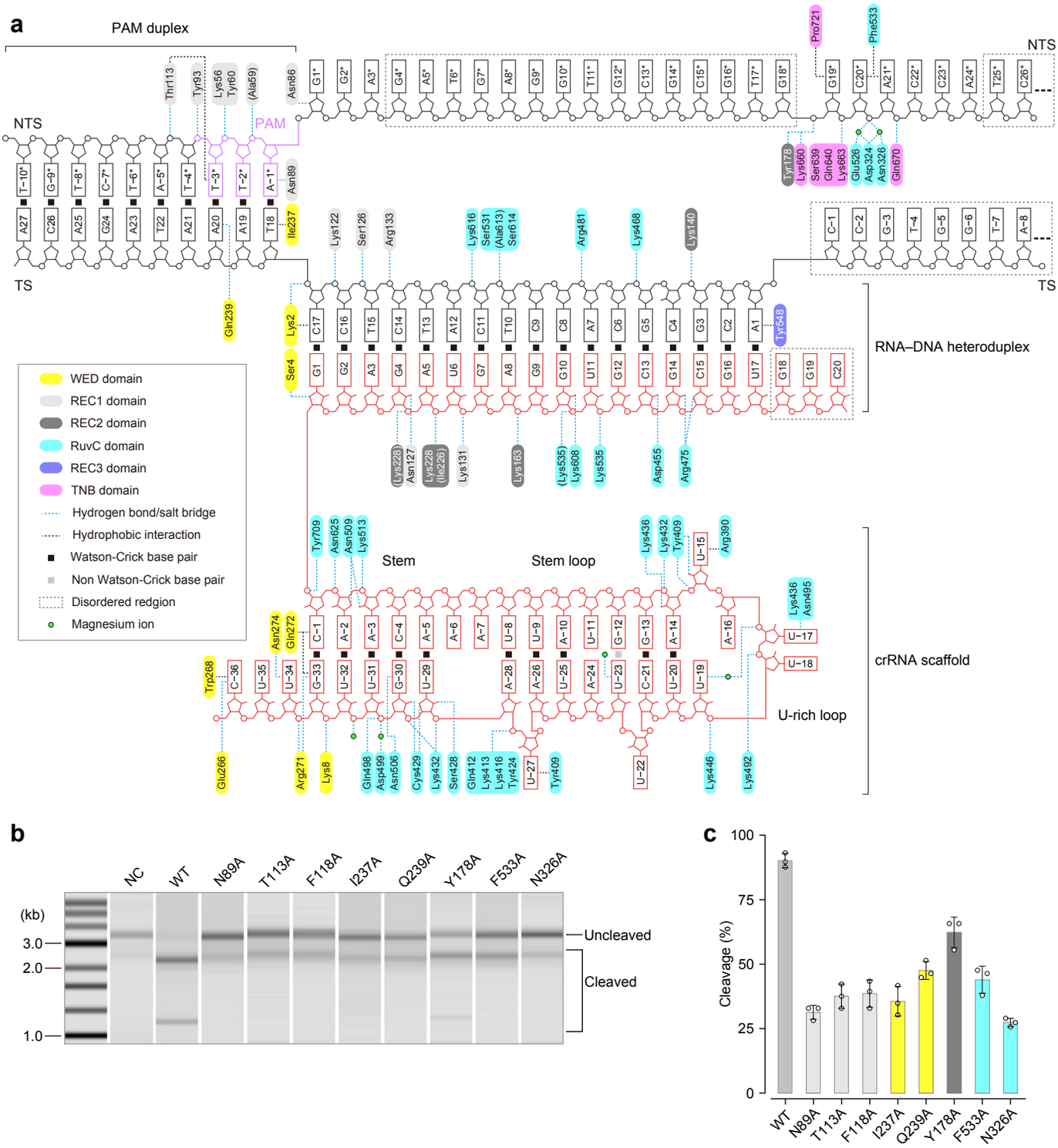

Supplementary Fig. 4 | Schematic of nucleic acid recognition.
(a) Residues that interact with nucleic acids through their main chains are shown in parentheses. The disordered regions are indicated by dashed gray lines.
(b) Representative electropherogram of DNA cleavage products analyzed by MultiNA microchip electrophoresis.
(c) In vitro DNA cleavage activities of WT Casλ2 and Casλ2 mutants. Data are mean ± s.d. (n = 3).

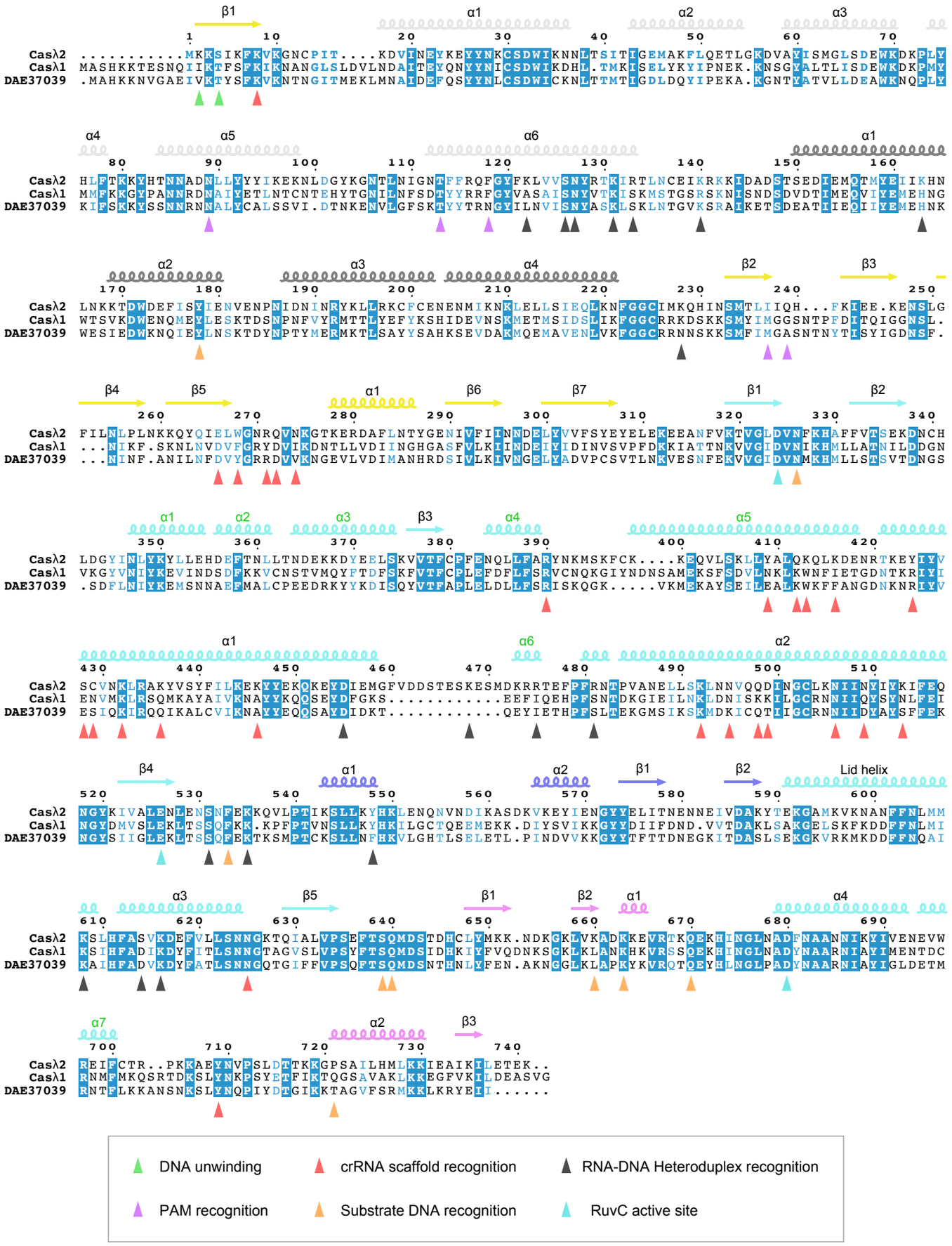

Supplementary Fig. 5 | Multiple sequence alignment of Casλ orthologues.
Multiple sequence alignment of Casλ1, Casλ2, and DAE37039 (a hypothetical protein from Bacteriophage sp. that demonstrated sequence similarity to Casλ2 in a BLAST analysis). The secondary structure of Casλ2 is indicated above the sequences. The additional helices observed in the RuvC domain of Casλ2 are numbered in green, as in Supplementary Fig. 3a. The key residues of Casλ2 are marked with triangles below the sequences. The figure was prepared using Clustal Omega (https://www.ebi.ac.uk/jdispatcher/msa/clustalo) and ESPript3 (https://espript.ibcp.fr/ESPript/ESPript/).

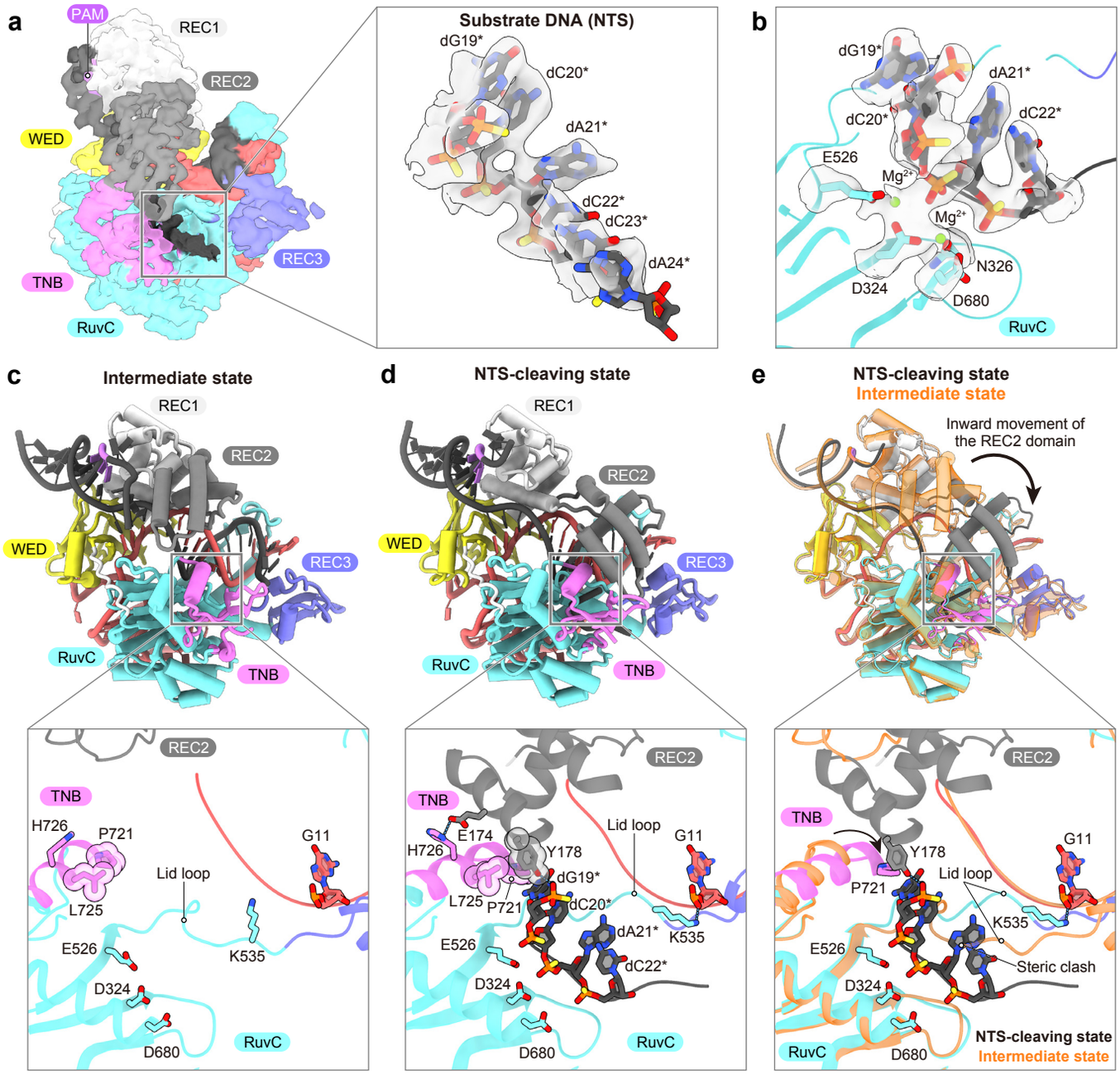

Supplementary Fig. 6 | Map-model superimposition and conformational changes of CasΛ2.
(a) Overall cryo-EM density map (left) and map-model superimposition of the substrate NTS bound within the RuvC active site (right).
(b) Close-up views of the RuvC active site of CasΛ2 in the NTS-cleaving state. Cryo-EM density maps are shown as translucent gray surfaces. The bound Mg2+ ions are shown as green spheres.
(c and d) Structures (top) and close-up views around the RuvC domain (bottom) of the CasΛ2–crRNA–target DNA complexes in the intermediate (**c**) and NTS-cleaving (**d**) states. Hydrogen bonds are shown as dashed lines.
(e) Superimposition of the intermediate (orange) and NTS-cleaving (colored as in d) states. The top and bottom panels display the overall structure and a close-up view around the RuvC active site, respectively. The inward movement of the REC2 domain toward the TNB domain is accompanied by the inward movement of a helix in the TNB domain toward the REC2 domain. The substrate NTS in the NTS-cleaving state clashes with the lid loop in the intermediate state.

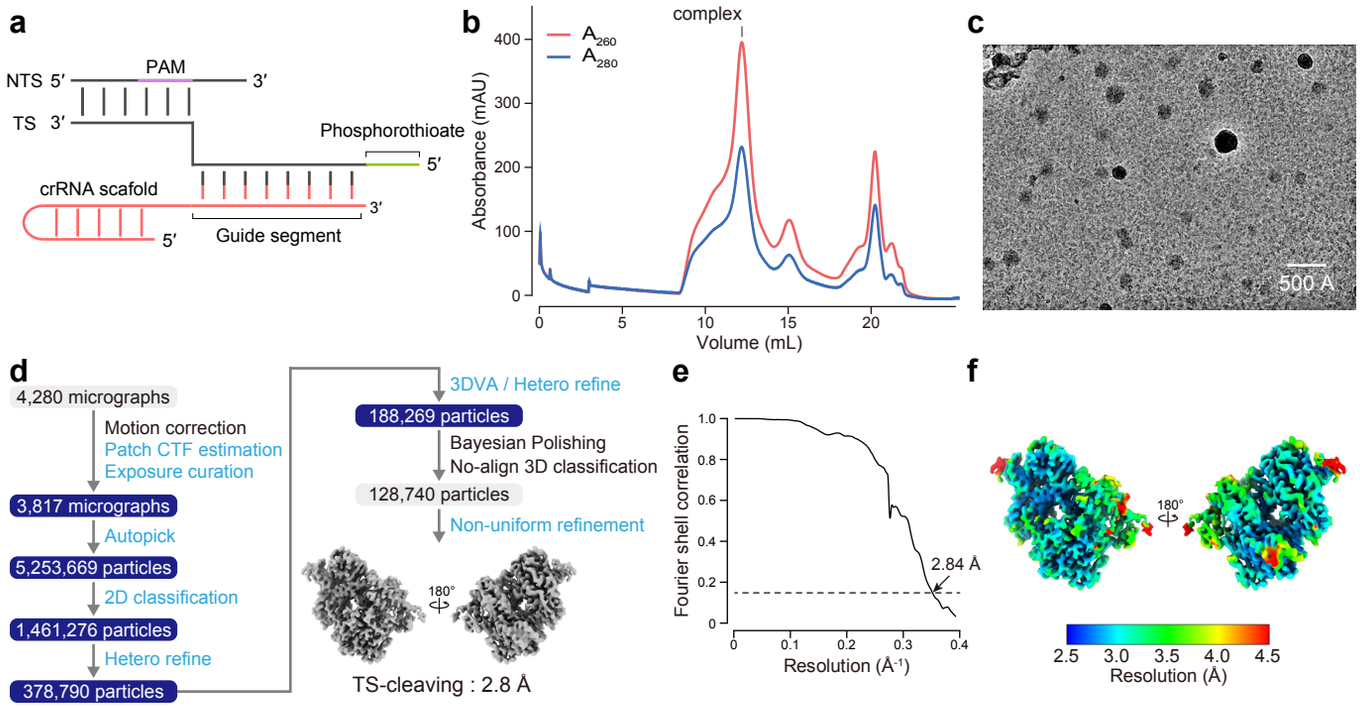

Supplementary Fig. 7 | Single-particle cryo-EM analysis of the Casλ2–crRNA–target DNA ternary complex in the TS-cleaving state.

(a) Schematic of the target DNA construct used in the complex reconstruction. Phosphorothioate modified regions in the target DNA strand are shown in green.

(b) Size-exclusion chromatography profile of the Casλ2–crRNA–target DNA complex in the TS-cleaving state. The peak fraction indicated as the complex was used for the following cryo-EM analyses.

(c) Representative cryo-EM micrograph, recorded on a 300-kV Titan Krios microscope with a K3 camera.

(d) Single-particle cryo-EM image processing workflow. The data processing done in cryoSPARC is shown in blue, while the processing done in RELION is shown in black.

(e) Fourier shell correlation curve for the 3D reconstruction.

(f) Cryo-EM density map according to the local resolution.

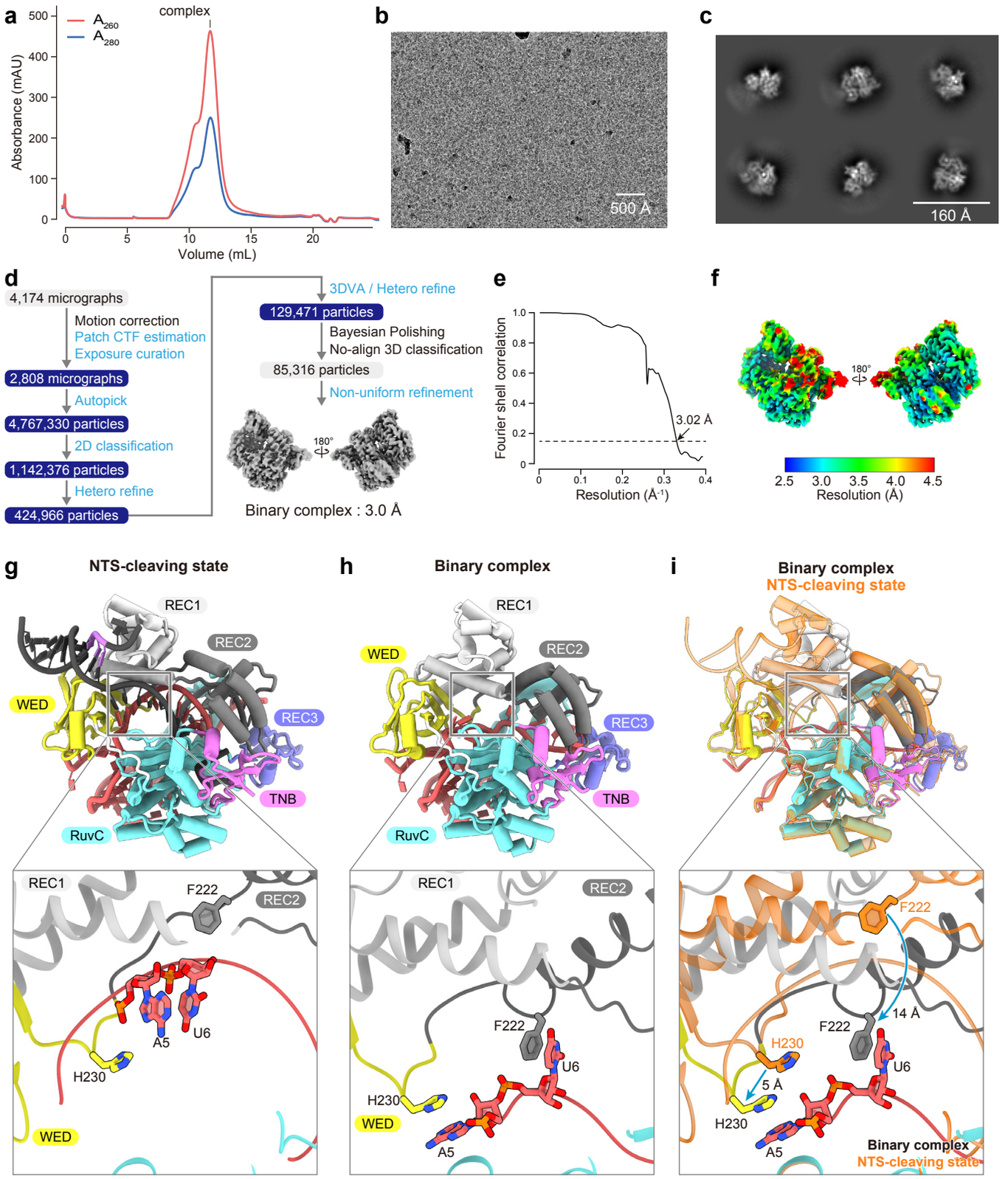

Supplementary Fig. 8 | Single-particle cryo-EM analysis of the dCasλ2–pre-crRNA binary complex.
(a) Size-exclusion chromatography profile of the dCasλ2–pre-crRNA complex. The peak fraction indicated as the complex was used for the following cryo-EM analyses.
(b) Representative cryo-EM micrograph, recorded on a 300-kV Titan Krios microscope with a K3 camera.
(c) Representative 2D class average images.
(d) Single-particle cryo-EM image processing workflow. The data processing done in cryoSPARC is shown in blue, while the processing done in RELION is shown in black.
(e) Fourier shell correlation curve for the 3D reconstruction.
(f) Cryo-EM density map according to the local resolution.
(g and h) Structures (top) and close-up views (bottom) of the Casλ2–crRNA–target DNA complex in the NTS-cleaving state (**g**) and the dCasλ2–pre-crRNA binary complex (**h**).
(i) Superimposition of the NTS-cleaving state (orange) and the binary complex (colored as in **h**). The top and bottom panels display the overall structure and a close-up view, respectively.

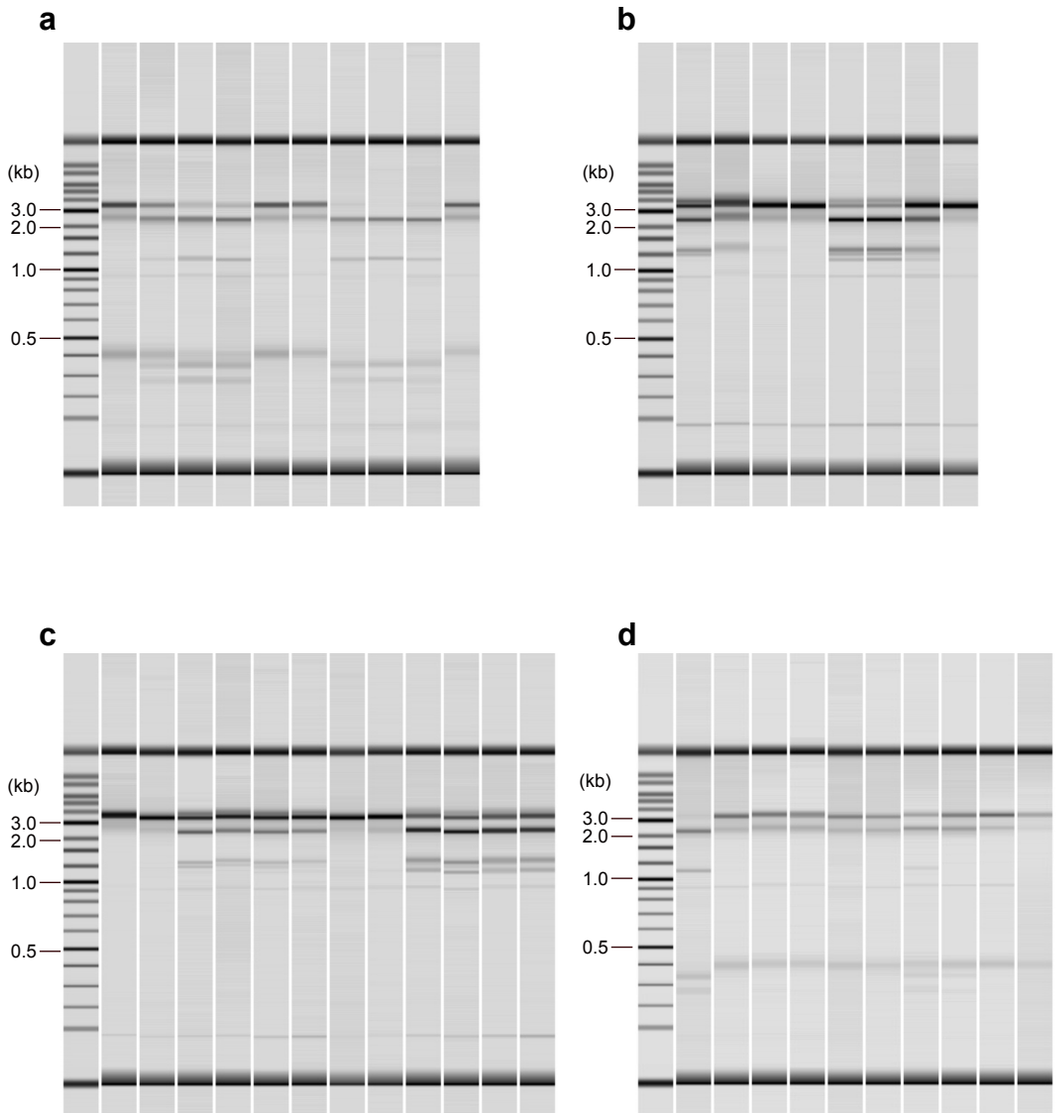

Supplementary Fig. 9 | Uncropped electropherograms.
(a–d) Uncropped electropherogram images used in Fig. 1e and Supplementary Fig. 1a (**a**), Fig.1f and Supplementary Fig. 1b (**b**), Fig.1g and Supplementary Fig. 1c (**c**), and Supplementary Fig.4b (**d**).

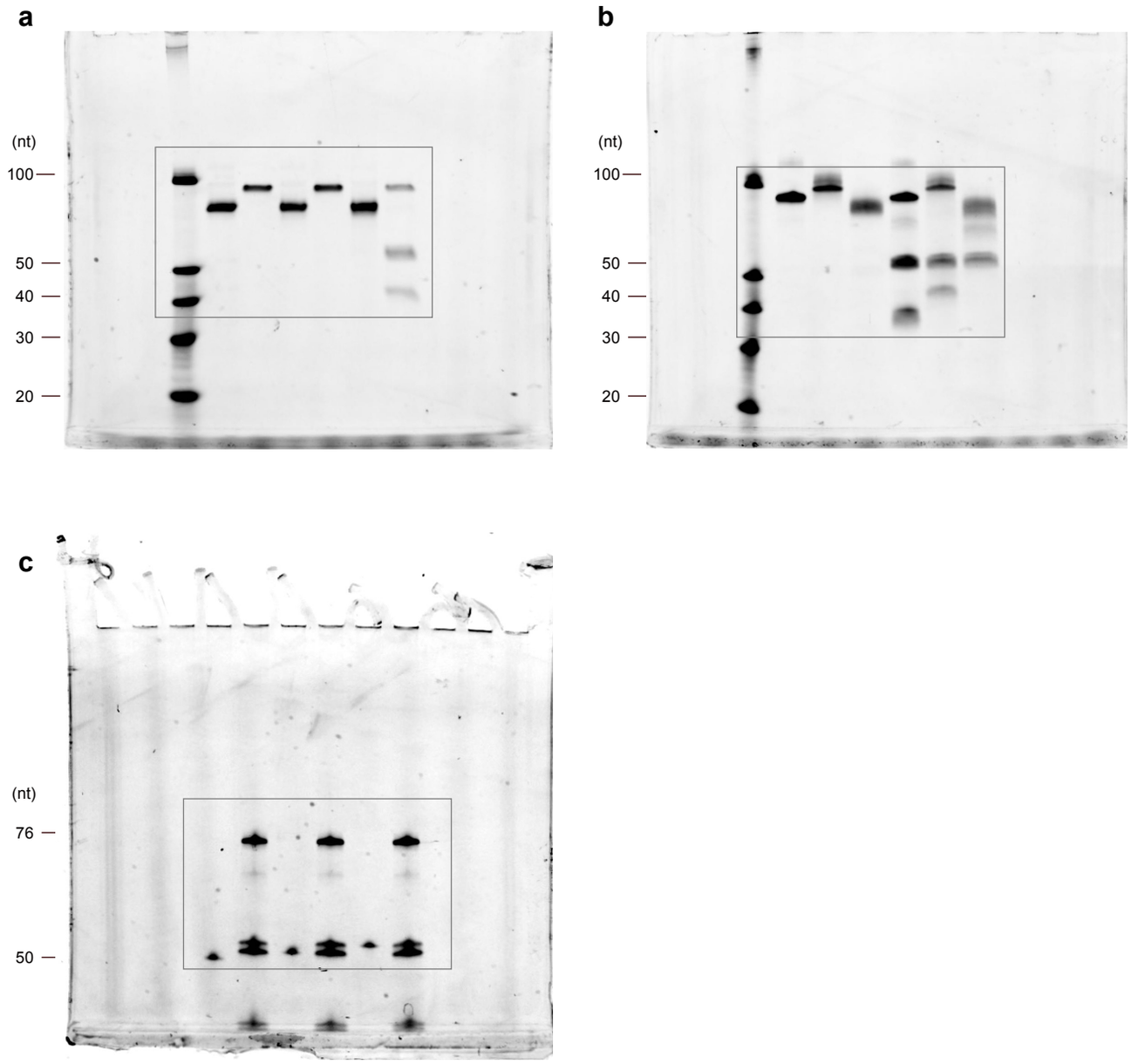

Supplementary Fig. 10 | Uncropped gel images.
(a–c) Uncropped gel images used in Fig. 5b (**a**), Fig.5d (**b**), and Fig.5e (**c**).

Primers used in this study.

Oligo	Sequence
RNA-T7-f	GGATCCTAATACGACTCACTATAGG
crRNA-r	GCCACGCGCACCTCATCTCCGTCTTGGCCTTCGCCCGCCAAGCTGGGCTA TGACACCCTATAGTGAGTCGTATTAGGATCC

Target DNA sequences used for the structural determination

Name	Sequence
Target DNA strand	GATGGTGCCACGCGCACCTCATCTCCCAAATAGACA
Non-target DNA strand	TGTCTATTTGGGAGATGAGGTGCGCGTGGCACCATC

Plasmid used for the structural determination

Name	Identifier
pE-His6-Casλ2	https://benchling.com/s/seq-6Go3ZmqGlRCNvmUgZ7vi?m=slm-EqjawmqpP5zxPR7wu2Fu

Supplementary Table S1. | Primers, target DNA sequences, and plasmids used in this study.